ADVANCED MATERIALS INTERFACES
Open Access
www.advmatinterfaces.de

Impact of Band-gap Gradient in Semi-Transparent and Bifacial Ultra-Thin $Cu(In,Ga)Se_2$ Solar Cells

*Christoph Rath, Yao Gao, Tristan Koehler, and Martina Schmid**

Ultra-thin $Cu(In,Ga)Se_2$ (CIGSe) solar cells on transparent conductive oxide back contact reduce the material consumption of rare indium and gallium and simultaneously exhibit great potential for semi-transparent bifacial application. For highly efficient CIGSe solar cells, a steep back Ga grading and Na treatment are expected. However, Na will promote the formation of highly resistive GaO_x at the rear interface owing to Ga accumulation. In this work, the three-stage co-evaporation process is renewed and the effect of the deposition sequence in the first stage on the Ga distribution as well as the cross-correlated influence of Na is explored. In particular, the standard deposition sequence of Ga+In is altered to start with In. When a thin In layer is pre-deposited on the back contact, the fill factor and efficiency increase. The deposition of In+Ga+In in the first stage of CIGSe growth leads to efficiencies 28% (on average) higher than for the standard deposition sequence of Ga+In. Additionally, 2.74% efficiency is reached under rear and 9.32% under simultaneous front and rear illumination. Therefore, adapting the deposition sequence in the first stage of CIGSe growth is identified as a key to improving the device performance on transparent back contact.

1. Introduction

Photovoltaics has taken the lead in the transition to power generation by renewables. Compared to the most established crystalline silicon technology, absorbers with direct band gaps get along with thicknesses in the µm range and thus allow lower material costs and flexible devices. Amongst these thin-film technologies, $Cu(In,Ga)Se_2$ or short CIGSe is a highly stable material that has achieved efficiency records up to 23.6%.[1] The standard thickness for the CIGSe absorber (2–2.5 µm) requires high consumption of scarce indium, and one strategy for lowering the manufacturing costs and enhancing the large-scale deployment is thinning down the absorber layer thickness to ultra-thin (500 nm).[2] Additionally, the fabrication of an ultra-thin CIGSe absorber can also shorten the deposition duration, which can reduce energy consumption and operation costs. So far, the champion efficiency of ultra-thin CIGSe solar cells (with a 490 nm absorber) is 15.2%.[3] Yet, due to the reduced absorber layer thickness, light absorption is incomplete and optical losses occur.[2b,4] As a result, the short circuit current density (J_{sc}) of ultra-thin CIGSe is significantly lower than for the standard thickness of a thin-film CIGSe solar cell and light-trapping concepts are employed to boost the absorption.[2b] The standard back contact of CIGSe solar cells is molybdenum (Mo), since a self-forming $MoSe_2$ layer evolves during the absorber deposition, resulting in an electrically beneficial quasi-Ohmic contact between the CIGSe absorber and the Mo back contact.[5] However, the parasitic absorption of the opaque Mo back contact increases the optical losses for ultra-thin CIGSe solar cells.[2c,6] As an alternative back contact, various transparent conductive oxides (TCOs) have been tested, such as tin-doped indium oxide (ITO), fluorine-doped tin oxide (FTO), and aluminum-doped zinc oxide (AZO).[6b,7] Compared to the opaque Mo back contact, CIGSe solar cells with a TCO back contact show promising application in semi-transparent, bifacial, or tandem solar cells.[7b,8] In other words, CIGSe on TCO back contact has the potential to improve the usage of unabsorbed light by reflecting it back into the absorber via a mirror on the rear side of the glass, by transmitting it to another application (e.g., bottom solar cell in a tandem) or by exploiting bifacial illumination (i.e., from both front and rear side of the solar cell).

In a CIGSe absorber, the band gap can be adjusted by changing the Ga/(Ga+In) (GGI) ratio.[9] Typically, the GGI ratio is higher on the back and near the front absorber surface, creating a U-shaped gradient.[9a,10] The stronger back gradient results in a wider band gap near the rear interface of the absorber compared to the bulk and still compared to the front surface, leading to a slightly higher valence band maximum (VBM) and a significantly higher conduction band minimum (CBM) there.[11] This rise in conduction band offset is beneficial to repel electrons from the back interface and move them toward the front surface of the

C. Rath, Y. Gao, T. Koehler, M. Schmid
Department of Physics and Center for Nanointegration Duisburg-Essen (CENIDE)
University of Duisburg-Essen
Forsthausweg 2, 47057 Duisburg, Germany
E-mail: martina.schmid@uni-due.de

The ORCID identification number(s) for the author(s) of this article can be found under https://doi.org/10.1002/admi.202400085

DOI: 10.1002/admi.202400085

absorber from where they will be extracted.[9b] Additionally, a slight increase in the GGI ratio at the front surface promotes the formation of a spike-like conduction band alignment at the CdS/CIGSe interface, which allows the electrons to move more easily to the CdS layer and thus reduces recombination.[12] However, an excessive Ga gradient can lead to a deterioration of the morphology and hence increase recombination.[13] Therefore, the optimization of the Ga-gradient is crucial.

In the commonly used three-stage co-evaporation process of CIGSe absorber fabrication, Ga and In are deposited in the first stage, and generally, the process starts with Ga.[2b,c,14] However, a highly resistive GaO_x layer can form at the CIGSe/ITO rear interface, especially during high-temperature deposition, which leads to blocking the hole extraction from the CIGSe absorber.[5] Absorber deposition at low substrate temperature is one approach to obtaining efficient semi-transparent CIGSe solar cells because the formation of the undesirable GaO_x at the CIGSe/ITO rear interface can be minimized.[2c] An alternative strategy to suppress the GaO_x formation is to pre-deposit an interface modification layer between the CIGSe absorber and the ITO back contact as it has been shown for the solution-based growth of CISSe.[15] The highest efficiency of a CIGSe solar cell (with standard absorber thickness) deposited on ITO back contact achieved 19.77%, and exploited a 15 nm thick pre-deposited Ag layer on the ITO back contact.[9b]

A further approach for performance enhancement of CIGSe solar cells is the treatment with alkali metals such as Na, K, and Rb, which can improve the open circuit voltage (V_{oc}).[16] Different strategies for alkali supply are researched for CIGSe: before, or after the absorber deposition. When the CIGSe absorber is deposited at high temperatures, Na will promote the formation of a highly resistive GaO_x layer at the CIGSe/TCO interface owing to Ga accumulation.[5] For CIGSe absorbers grown by co-evaporation, the most commonly applied configuration is alkali post-deposition treatment (PDT), that is, the supply of NaF in a fourth stage and in presence of selenium.[16,17] Sodium fluoride (NaF) PDT has been widely applied for alkali incorporation, as it was identified to affect the grain size, crystal orientation, and p-type conductivity.[2c,16b] The Na atoms can passivate the CIGSe grain boundaries, and simultaneously occupy the Cu vacancies of the CIGSe surface.[18] Consequently, Na_{Cu} defects are formed, leading to a high Na concentration at the front surface. However, an excessively high Na concentration near the front surface of the absorber hinders the formation of the Cd_{Cu} donor defect during the CdS CBD deposition, resulting in a degraded pn-junction.[18,19] Therefore, the NaF content for alkali treatment should be controlled. By fine-tuning the NaF PDT we have fabricated over 12% efficient ultra-thin CIGSe solar cells on ITO back contact before.[2c] NaF pre-deposition (Pre-DT) is an alternative process for alkali treatment.[20] The Na_2Se_x, which is mainly located at the grain boundaries, acts as a Se reservoir during CIGS grain growth, passivating defects and filling Cu vacancies, thus increasing the p-type carrier concentration and V_{oc}.[21]

In this research, we alter the standard deposition sequence during the first stage of the CIGSe co-evaporation process to achieve a slightly In-rich rear interface and a band-gap gradient supporting carrier extraction: Whereas the first stage generally starts with Ga for the purpose of back Ga gradient formation, we newly introduce an initial step of In evaporation. The CIGSe absorbers are deposited at a low substrate temperature (first stage at 410 °C, second and third stage at 450 °C) to minimize GaO_x formation already from the beginning. The CIGSe absorbers are deposited on ITO and for comparison on Mo back contact. In addition, NaF is utilized for alkali treatment by PDT and Pre-DT processes. The position of the maximum GGI value in the absorber significantly affects the photovoltaic (PV) performance of the CIGSe solar cells and will be tuned by the sequence of elements offered in the first stage of the absorber growth.

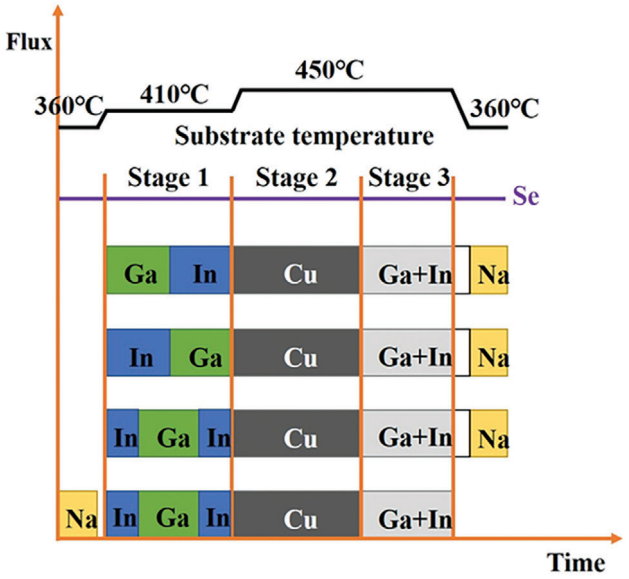

Figure 1. CIGSe absorber deposition by a three-stage co-evaporation process with various strategies of In and Ga supply in the first stage.

2. Results

To tune the band-gap gradient, which is affecting the electron and hole transport, we designed three different deposition sequences in the first stage of the CIGSe absorber growth. For the reference CIGSe absorber, first Ga then In was deposited during the first stage (Ga+In CIGSe, top line of **Figure 1**). To introduce a thin Ga-poor layer directly at the back contact, we altered the deposition sequence in the first stage and initially supplied In followed by Ga (In+Ga CIGSe, second line in Figure 1). With the aim of keeping the Ga-poor area minimal, we further altered the first stage to provide shortly In, then Ga, then In again (In+Ga+In CIGSe, third line in Figure 1). NaF PDT was utilized for Na incorporation into the CIGSe absorbers fabricated by these three recipes. In addition, the NaF Pre-DT was tested for the In+Ga+In strategy, described as Na+In+Ga+In CIGSe (bottom line in Figure 1).

The GD-OES results for the CIGSe absorbers deposited on Mo back contact with various deposition strategies in the first stage are shown in **Figure 2**. Corresponding composition depth profiles and a comparison of the individual element profiles of these absorbers are displayed in Figures S1 and S2 (Supporting Information), respectively. Generally, the CIGSe absorbers

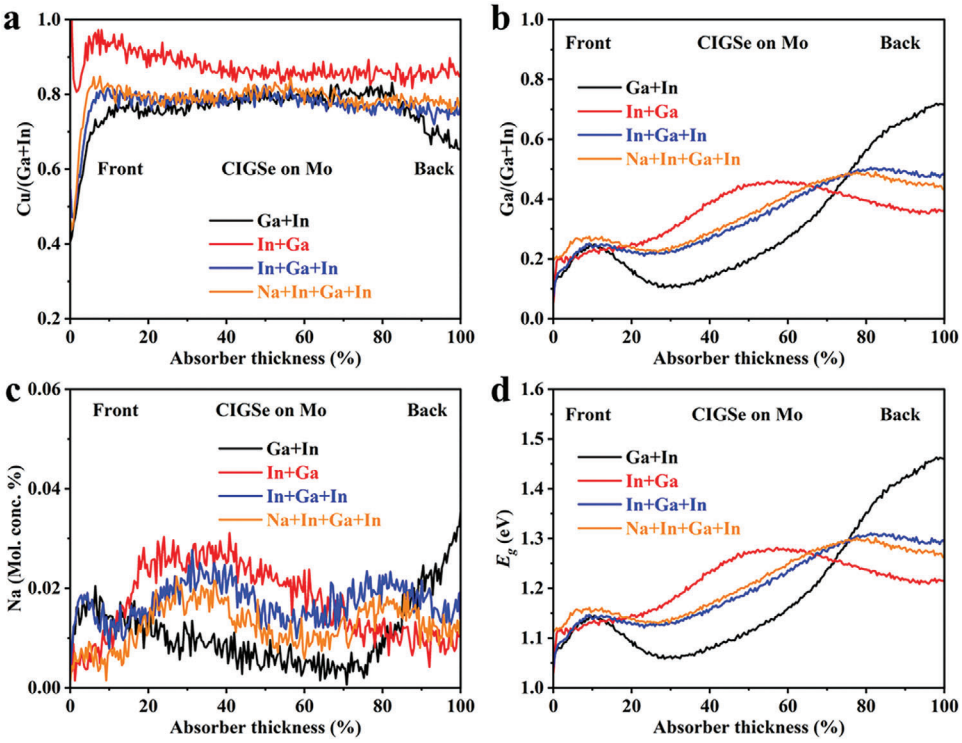

Figure 2. a) Cu/(Ga+In) ratios, b) Ga/(Ga+In) ratios, c) Na molar concentration, and d) band gap of CIGSe absorbers deposited on Mo back contact with various deposition strategies in the first stage as measured by or derived from GD-OES. The *x*-axis is normalized to 100% absorber thickness.

exhibit a Cu-poor front surface, which is beneficial to form a high-quality pn-junction with CdS and the ZnO layers (Figure 2a). The In+Ga CIGSe, however, shows an increase in CGI ratio at the immediate front surface, which is related to a lower-quality pn-junction because of hindered Cd^{2+} diffusion during the CdS CBD process.[18,22] Furthermore, the CGI across the entire absorber is higher for In+Ga CIGSe compared to the other samples. A U-shaped GGI ratio with a minimum in the first third from the front interface and a maximum in the second half is observed for all CIGSe absorbers (Figure 2b). In more detail, it can also be regarded as a W-shape since there are additional minima at the very front and rear positions. The maximum GGI value of Ga+In CIGSe is located at the rear side of the absorber. No matter, if NaF PDT or NaF Pre-DT is applied, for (Na+)In+Ga+In CIGSe, the maximum GGI values are found close to 80% absorber depth. On the contrary, the maximum GGI value of In+Ga CIGSe shifts to 50% absorber depth. The Ga+In and In+Ga+In CIGSe with NaF PDT display—as expected—a higher Na concentration near the front surface (0%–20% depth) than the NaF Pre-DT sample (Na+In+Ga+In) (Figure 2c). This observation is in line with reports that Na atoms can occupy Cu vacancies to form Na_{Cu} defects.[18,19] For the In+Ga CIGSe with NaF PDT, however, a high Cu concentration was found at the front surface (Figure S2, Supporting Information) resulting in a significantly lower Na concentration than for Ga+In and In+Ga+In CIGSe. Interestingly, a very pronounced rise of the Na content toward the rear interface is observed for Ga+In CIGSe (rather than for Na+In+Ga+In). This finding can directly be correlated with the high Ga content at the rear interface linked to small grains with many grain boundaries where the Na can accumulate.[2c,13,23]

Band gap grading profile of these CIGSe absorbers can be calculated from the elemental distribution based on the following equation:[24]

$$E_g\ (x,y) = \left(1.00 + 0.13x^2 + 0.08x^2y + 0.13xy + 0.55x + 0.54y\right)\ eV \quad (1)$$

where *x* and y are Ga/(Ga+In) and S/(S+Se) ratio, respectively. In our experiment, sulfur is absent and $y = S/(S+Se) = 0$. Therefore, the band gap of these CIGSe absorbers depends on the GGI ratios only and a close correlation is found (compare Figure 2b,d). $CuInSe_2$ ($E_g = 1.04$ eV) and $CuGaSe_2$ ($E_g = 1.68$ eV) have a similar valence band maximum (VBM).[11a] The conduction band minimum (CBM), however, shifts toward the vacuum level by increasing the GGI ratio, indicating that the CBM of $CuGaSe_2$ is closer to the vacuum level than that of $CuInSe_2$.[11] Therefore, the band gap of the CIGSe absorber is widened with increasing GGI ratio. In other words, the band gap profile in a CIGSe absorber is determined by the depth-dependent CBM resulting from the GGI distribution. The maximum GGI of Ga+In CIGSe is closer to the rear interface than for the other samples, implying that the Ga+In CIGSe has a steep band-gap grading and a significantly higher CBM toward the rear interface. The electrons are transported from the high to the low CBM, that is, away from the back contact.[11b] In contrast, the GGI result of In+Ga CIGSe shows a peak-like band gap (or CBM) profile, in which the maximum GGI value is observed at ≈ 50% absorber depth. The photo-generated electrons in the bottom absorber region flow to the rear interface direction, whereas the photo-generated electrons in the front region flow toward the front surface.[25] This peak-like band gap profile thus hinders the electron transport and exhibits a severe

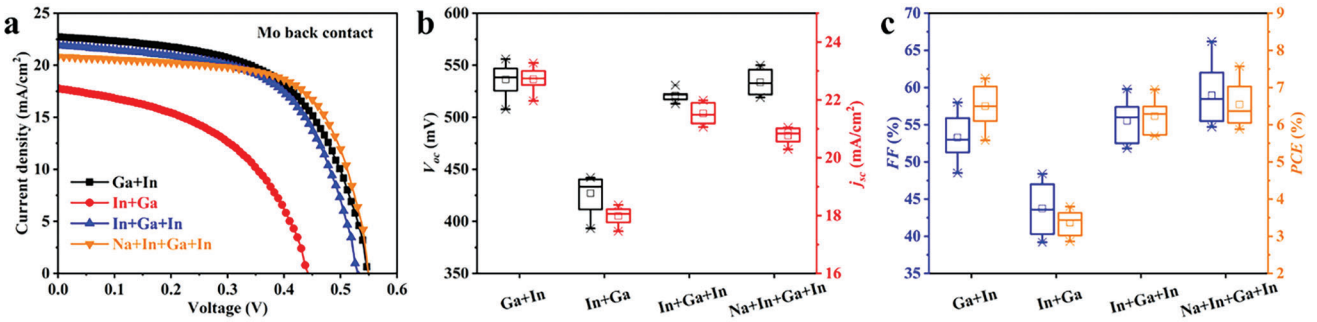

Figure 3. a) *J–V* curves of the best CIGSe solar cells on Mo back contact fabricated by various deposition strategies in the first stage of the absorber growth. Statistical distribution of b) open circuit voltage V_{oc} and short circuit current density J_{sc}, and c) fill factor *FF* and power conversion efficiency *PCE* derived from 10 devices for each strategy.

shunting behavior,[25] since the photo-generated electrons in the bottom region of the In+Ga CIGSe absorber cannot be extracted effectively.

Figure 3 presents the current density–voltage (*J–V*) curves of the best CIGSe solar cells on Mo back contact from various deposition strategies in the first stage of the absorbers growth. The best Ga+In CIGSe solar cell of this series exhibits a 7.25% efficiency, with a V_{oc} of 549.5 mV, a J_{sc} of 22.72 mA cm^{-2}, and a *FF* of 58.0%. When In+Ga is deposited in the first stage, all the PV parameters of the best device significantly decrease as compared to the best Ga+In CIGSe solar cell (Figure 3 and **Table 1**). The best efficiency of In+Ga is significantly reduced to 3.80%. The degraded PV performance can be linked to the band gap profile, see the explanations related to Figure 2d. The In+Ga+In samples show a reduction of V_{oc} and J_{sc} but an improvement of *FF* and efficiency compared to Ga+In CIGSe. Maximum efficiencies of 6.95% and 7.57% are reached for In+Ga+In with NaF PDT and NaF Pre-DT, respectively. The higher efficiency of the NaF Pre-DT CIGSe device (Na+In+Ga+In) can be explained by the growth of an electrically favorable $MoSe_2$ interlayer at the rear interface promoted by the Na.[2c,19a]

Figure 3b,c shows the statistical distributions of the PV parameters for the CIGSe solar cells on Mo (10 CIGSe sub-cells) with absorbers from various deposition strategies (summarized also in Table 1). These PV parameters reveal the same trends as the corresponding highest-efficient CIGSe solar cells. It is indicated that the In+Ga+In and Na+In+Ga+In CIGSe can obtain similar efficiency as the Ga+In sample. The In+Ga+In samples, both with NaF Pre-DT and PDT, show the potential to achieve highly efficient CIGSe solar cells on Mo back contact with the maximum efficiency reached for Na+In+Ga+In.

Table 1. Electrical parameters of CIGSe on Mo back contact with various deposition strategies in the first stage.

Sample	V_{oc} [mV]	J_{sc} [mA cm^{-2}]	*FF* [%]	Efficiency [%]
Ga + In	536.36 ± 14.76	22.71 ± 0.42	53.27 ± 3.01	6.50 ± 0.56
	549.5	22.72	58.0	7.25
In + Ga	427.0 ± 16.59	17.98 ± 0.32	43.73 ± 3.47	3.36 ± 0.34
	442.1	17.77	48.4	3.80
In + Ga + In	520.95 ± 4.79	21.53 ± 0.36	55.53 ± 2.72	6.23 ± 0.42
	530.8	21.90	59.8	6.95
Na + In + Ga + In	533.51 ± 12.67	20.76 ± 0.27	58.96 ± 3.79	6.54 ± 0.59
	549.4	20.82	66.2	7.57

External quantum efficiency (EQE) spectra of these best-performaning CIGSe devices are depicted in Figure S3a (Supporting Information). They show a similar behavior in the short wavelength range (300–390 nm). The Ga+In CIGSe exhibits a significantly higher spectral response from 540 to 1200 nm wavelength than CIGSe from the other strategies, leading to a higher J_{sc} of the Ga+In CIGSe device. The band gap (E_g) values of these CIGSe absorbers are extracted from the plot of $[E\times\ln(1-EQE)]^2$ versus *E* (Figure S3b, Supporting Information).[15] The Ga+In CIGSe presents a smaller E_g value (1.03 eV) than the other three types of CIGSe in agreement with the slightly higher J_{sc} of the Ga+In CIGSe solar cell (Figure 3a). This E_g extracted from EQE is linked to the minimum value of the E_g profile (Figure 2d),[24b] because the semiconductor materials can only absorb light starting from the band gap energy. The Urbach energies of the CIGSe absorbers can be extracted by fitting the slope of the ln(EQE) spectrum at the long-wavelength edge.[26] It is reported that E_U impacts the carrier mobility and lifetime of the absorbers as well as the open-circuit voltage deficit of thin film solar cells.[26] Theoretically, a small E_U value implies a high quality of the absorber as well as a high carrier mobility and lifetime, resulting in high photovoltaic performance.[26a] The In+Ga CIGSe solar cell owns a larger E_U value (22.71 meV) than those from the other three deposition strategies (Figure S3c, Supporting Information), which can explain the low efficiency of the In+Ga device (Figure 3a and Table 1). However, the Na+In+Ga+In CIGSe solar cell exhibits the best efficiency (Figure 3a and Table 1) and smallest E_U value (16.03 meV, Figure S3c, Supporting Information), indicating that the rear interface modification is a potential strategy for achieving high-performance CIGSe solar cells.

For the semi-transparent solar cells on ITO back contact, the GD-OES results of the CIGSe absorbers with various deposition strategies in the first stage are shown in **Figure 4**. Corresponding composition depth profiles and a comparison of the individual element profiles of these absorbers are displayed in Figures S4 and S5 (Supporting Information), respectively. All these CIGSe absorbers exhibit a Cu-poor composition (CGI < 1, Figure 4a). In addition, the CGI ratio at the front surface of the absorbers is lower than in the absorber bulk, which can be explained by the formation of the $Cu(In,Ga)_3Se_5$ ordered vacancy compound.[11b]

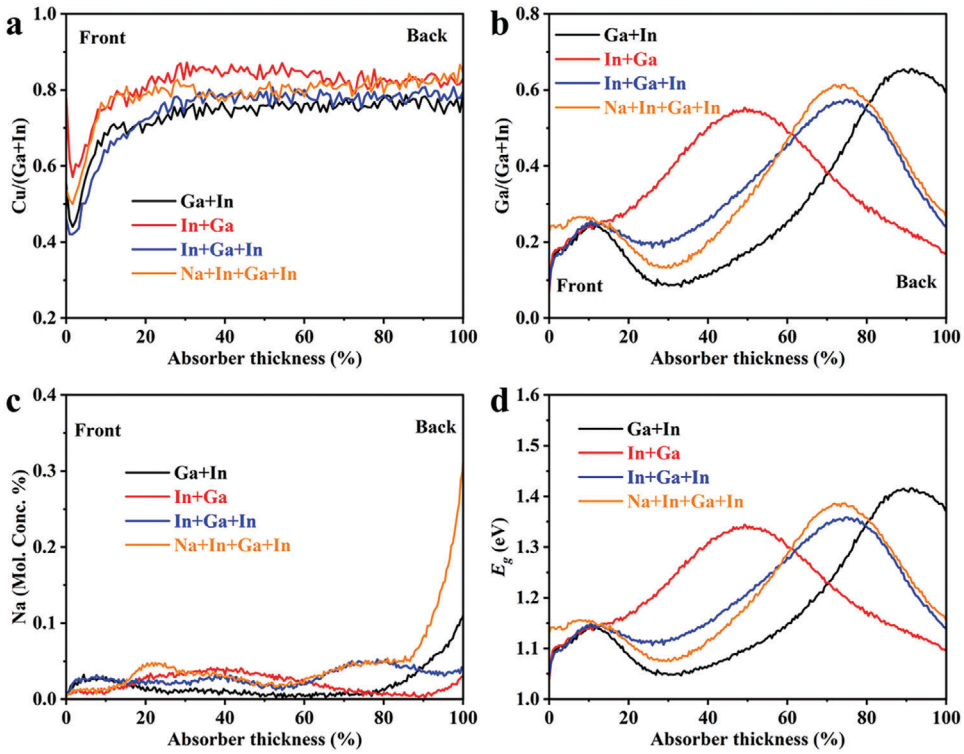

Figure 4. a) Cu/(Ga+In) ratios, b) Ga/(Ga+In) ratios, c) Na concentration, and d) band gap of CIGSe absorbers on ITO with various deposition strategies in the first stage measured by or derived from GD-OES. The *x*-axis is normalized to 100% absorber thickness.

The In+Ga CIGSe shows the highest CGI, also at the front surface, just as observed on the Mo substrate coated in the same process (Figure 2a). This observation implies that the In+Ga absorber has fewer Cu vacancies than Ga+In, In+Ga+In, and Na+In+Ga+In CIGSe.

The GGI ratios of the various CIGSe absorbers present a W-shaped Ga gradient.[10] In other words, starting from the front surface, the GGI ratio first shows an increase followed by a slight decrease, and then increases further toward the rear interface where it drops again (Figure 4b). For the Ga+In CIGSe absorber, the maximum GGI ratio is reached near the rear interface, resulting from the Ga accumulation.[13] Compared to Ga+In CIGSe, a slight shift toward the front surface of the maximum GGI ratio is observed for both In+Ga+In and Na+In+Ga+In CIGSe, owing to the initial deposition of In in the first stage. With increasing time of initial In deposition as conducted for In+Ga CIGSe, the maximum GGI ratio is found in the middle of the absorber.

The Na concentrations of these CIGSe absorbers are shown in Figure 4c. Compared to In+Ga and Na+In+Ga+In CIGSe, higher Na concentrations are observed for the Ga+In and the In+Ga+In samples near the front surface (0%–18% of absorber thickness). It is implied that a larger number of Cu vacancies are occupied by Na to form Na_{Cu} defects at the surface of the Ga+In and In+Ga+In CIGSe absorbers. According to literature, the Na atoms of Na_{Cu} defects can be replaced by Cd^{2+} to format Cd_{Cu} donor defects during the CdS CBD process, leading to a better quality of the pn-junction.[18,19] The excess Na at the front surface is released into the water.[18,19b] The Na concentrations increase near the rear interface, especially in the Ga+In and Na+In+Ga+In absorbers. With increasing GGI (0.3–0.76) at the rear interface, the CIGSe grains at the bottom of the absorber become smaller.[13,19b] Na atoms can occupy the grain boundaries of these small CIGSe grains, leading to a higher Na concentration.[19b,21b]

The maximum band gap value of Ga+In CIGSe is close to the rear interface (90% absorber depth, Figure 4d), implying a steep Ga grading toward the back contact. When the deposition sequence in the first stage is In+Ga, the maximum band gap value and hence the highest CBM are observed at 50% absorber depth. Therefore, the photo-generated electrons in the bottom region of In+Ga CIGSe are hindered from migrating toward the front and thus cannot be separated effectively.[9b] The In+Ga+In and Na+In+Ga+In CIGSe absorbers display a similar band gap distribution, yet, with the maximum values at 75% absorber depth and thus closer to the rear interface.

The PV parameters of the CIGSe solar cells on ITO back contact reveal maximum efficiencies of 5.71%, 2.84%, 6.18%, and 5.15% for Ga+In, In+Ga, In+Ga+In, and Na+In+Ga+In CIGSe devices, respectively (**Figure 5a** and **Table 2**). The best efficiency is thus achieved for the In+Ga+In sample confirming that a slight addition of In at the rear interface is beneficial for achieving high-quality CIGSe solar cells. Comparing the best CIGSe devices, the V_{oc}, J_{sc}, and efficiency decrease for In+Ga compared to the Ga+In CIGSe device. The reduction of the PV parameters can be attributed to the maximum GGI being located in the bulk of the absorber rather than near the rear interface, leading to a barrier for the electron transport (Figure 4b). Even though the J_{sc} of the In+Ga+In CIGSe device is smaller than for Ga+In CIGSe,

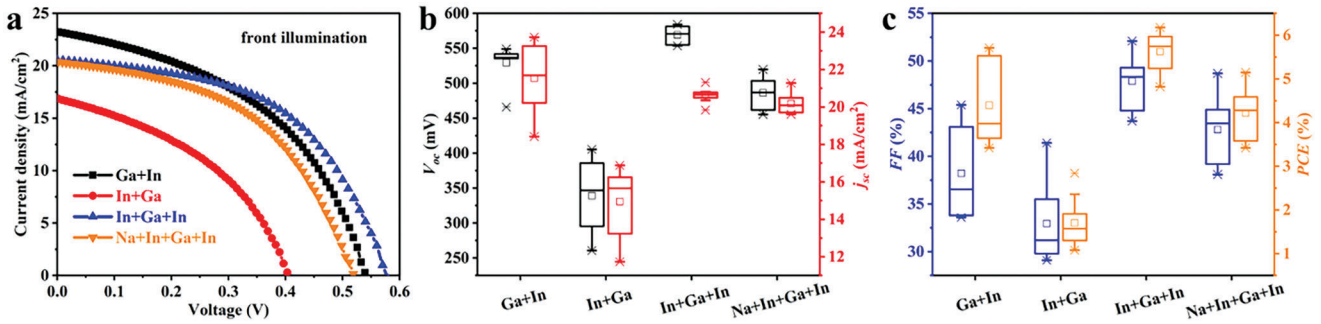

Figure 5. a) *J–V* curves of the best CIGSe solar cells on ITO back contact by various deposition strategies in the first stage for the absorber. Statistical distribution of b) open circuit voltage V_{oc} and short circuit current density J_{sc}, and c) fill factor *FF* and power conversion efficiency *PCE* derived from 10 devices for each strategy.

V_{oc}, *FF*, and efficiency are higher. A lower PV performance is observed for In+Ga+In with Pre-DT compared to NaF PDT because the initial addition of Na catalyzes the GaO_x interlayer formation on ITO. The GaO_x leads to a larger series resistance (1.23 Ω cm^2 for Na+In+Ga+In and 0.97 Ω cm^2 for In+Ga+In, see Figure S6, Supporting Information), which hinders the separation and transport of photo-generated carriers.[5,25] Thus, for ITO substrates, PDT is superior to Pre-DT for Na incorporation into ultra-thin CIGSe absorbers.

The statistical distributions of the PV parameters for the CIGSe solar cells on ITO (10 CIGSe sub-cells) with the absorbers obtained from various deposition strategies in the first stage are visualized in Figure 5b,c (and summarized in Table 2). These PV parameters show the same trends as the highest-efficient CIGSe solar cells with the maximum efficiency for the In+Ga+In sample related to the significantly increased V_{oc} and *FF*. Additionally, all the PV parameters of the In+Ga+In CIGSe solar cells present smaller error bars as compared to Ga+In CIGSe (Figure 5b,c and Table 2), indicating that this proposed novel deposition sequence in the first stage cannot only lead to improved efficiency but also to higher reproducibility.

EQE spectra of the semi-transparent CIGSe solar cells are displayed in Figure S7a (Supporting Information). These EQE spectra reveal a comparable behavior to those of CIGSe on Mo back contact. In detail, these semi-transparent CIGSe solar cells have a similar EQE spectral response from 300 to 390 nm wavelength. Furthermore, the Ga+In CIGSe exhibits a significantly higher spectral response from 540 to 1200 nm wavelength than CIGSe of the other strategies, which can explain a higher J_{sc} of the Ga+In CIGSe device. The In+Ga+In and Na+In+Ga+In CIGSe present an overlapping EQE spectrum, leading to similar J_{sc} values (Table 2). Compared to CIGSe solar cells on Mo back contact, these semi-transparent CIGSe exhibit an overall larger E_g (Figure S7b, Supporting Information). Simultaneously, the Ga+In CIGSe presents a smaller E_g value (1.09 eV) than the other three types of CIGSe in correlation with a slightly higher J_{sc} of the Ga+In CIGSe solar cells. The semi-transparent CIGSe solar cells exhibit larger E_U values than the Mo-based ones (Figure S7c, Supporting Information, compared to Figure S3c, Supporting Information). Simultaneously, the values are also higher than the thermal energy at room temperature (≈ 25 meV = k_BT, with k_B the Boltzmann constant and *T* the temperature), indicating low carrier mobility and lifetime.[16a,26] It is reported that lower Urbach energies reflect the improved transport of carriers.[16a,27] However, the Urbach energies are equally affected by lattice vibrations and defects,[26c] structural disorder,[27] alkali incorporation,[26b] and CGI ratio.[16a] Finally, also the CIGSe growth on semi-transparent back contacts may impact the absorber and the Schottky contact the carrier transport. Therefore, the relationship between Urbach energies and photovoltaic performance of semi-transparent CIGSe solar cells is still to be explored in the future.

Table 2. PV performance parameters (front illumination) of CIGSe on ITO back contact with various deposition strategies in the first stage.

Sample	V_{oc} [mV]	J_{sc} [mA cm^{-2}]	*FF* [%]	Efficiency [%]
Ga + In	529.19 ± 25.45	21.53 ± 1.74	38.20 ± 4.76	4.39 ± 0.95
	541.1	23.26	45.4	5.71
In + Ga	338.93 ± 51.92	14.94 ± 1.94	32.93 ± 4.17	1.70 ± 0.55
	405.4	16.88	41.4	2.84
In + Ga + In	569.14 ± 12.22	20.62 ± 0.37	47.87 ± 2.83	5.62 ± 0.45
	577.4	20.56	52.1	6.18
Na + In + Ga + In	486.24 ± 22.61	20.18 ± 0.55	42.79 ± 3.69	4.22 ± 0.61
	519.9	20.37	48.7	5.15

The bifacial *J–V* measurements are carried out three months after the standard *J–V* measurements. The then measured *J–V* curves under front and rear illumination of the formerly best CIGSe solar cells deposited on ITO back contact are shown in **Figure 6a**. From the front illumination measurement, we observe that all CIGSe solar cells, which were kept in ambient condition for three months, present an increase in J_{sc} (**Table 3**). This may be attributed to the formation of a thin In_2S_3 layer at the CdS/CIGSe interface with time, owing to the small standard molar enthalpy of formation of In_2S_3 or $In_2(O,S)_3$.[37] However, the CIGSe solar cells with NaF PDT exhibit a *FF* reduction (Table 3), in contrast to the stable *FF* for CIGSe with NaF Pre-DT. Compared to the fresh measurement, the re-measured Ga+In and In+Ga+In CIGSe solar cells present reductions in V_{oc} and efficiency (Table 3). On the contrary, an improvement of these PV parameters is observed for the In+Ga and Na+In+Ga+In CIGSe solar cells.

When comparing the highest efficient CIGSe devices obtained from different deposition strategies in the first stage of absorber growth under rear and front illumination, similar trends are

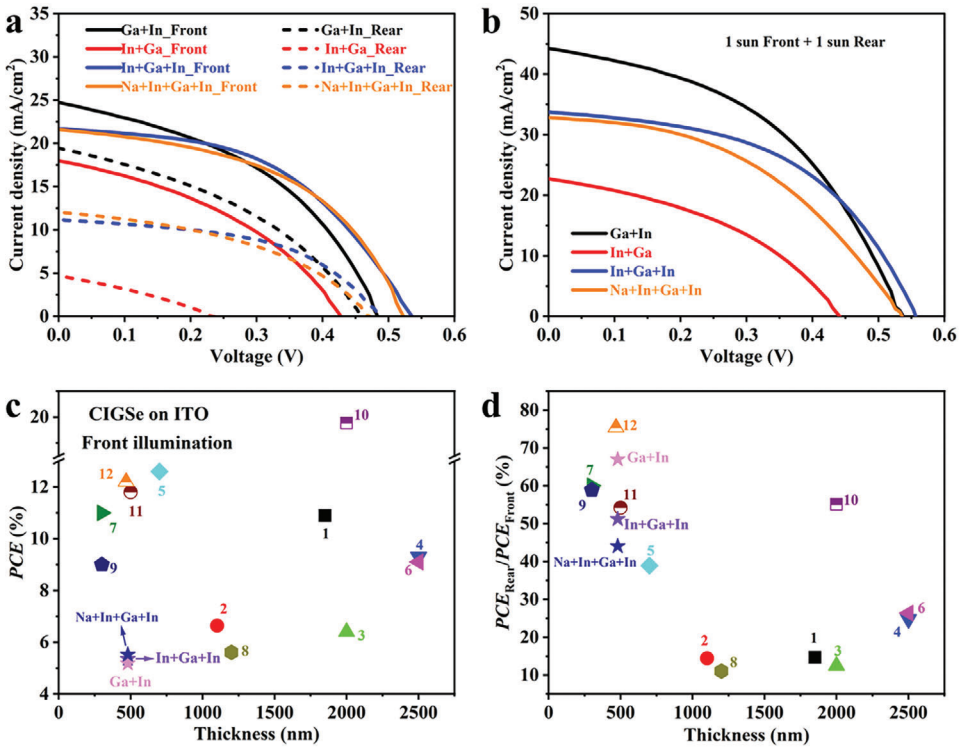

Figure 6. a) *J–V* curves of CIGSe on ITO with either front or rear illumination, b) *J–V* curves of semi-transparent CIGSe solar cells with simultaneous front illumination and rear illumination. c) The efficiency of state-of-the-art bifacial CIGSe solar cells under front illumination, d) the ratios of front illuminated efficiency/ rear illuminated efficiency. Mazzer et al.,[28] Chu et al.,[29] Nishimura et al.,[30] Mavlonov et al.,[31] Nakada et al.,[32] Mavlonov et al.,[33] Shin et al,[34] Moon et al.,[35] Shin et al,[7b] Yang et al.,[9b] Li et al.,[36] and Li et al.[8a]

found (Figure 6a). However, when the CIGSe devices are measured under the rear illumination, the PV parameters are significantly lower than for front illumination. This performance reduction under rear illumination mainly results from the drop in J_{sc}, which can be attributed to a lower charge-collection efficiency.[7b] The high rear contact recombination leads to a decrease in charge collection, resulting in performance loss in the semi-transparent CIGSe devices under rear illumination.[7b,8] The highest rear-illuminated efficiency (3.47%) is achieved by the Ga+In CIGSe solar cell. The In+Ga+In devices, both with NaF PDT and Pre-DT, present lower efficiencies (2.74% and 2.43%, respectively) due to the remarkably lower J_{sc} (11.19 and 12.06 mA cm^{-2} for In+Ga+In and Na+In+Ga+In compared to 19.43 mA cm^{-2} for Ga+In). The rear illumination efficiency of the In+Ga CIGSe device is negligible (0.34%), resulting from severe drops in all PV parameters. Interestingly, for the In+Ga+In CIGSe device, the *FF* improves under rear illumination, underlining the high quality rear-contact formation.

Table 3. Best PV performance parameters of CIGSe on ITO back contact under front or rear illumination, and bifacial illumination.

Sample		V_{oc} [mV]	J_{sc} [mA cm^{-2}]	*FF* [%]	Efficiency [%]
Ga + In	Front illumination	483.5	24.74	43.3	5.18
	Rear illumination	458.3	19.43	38.9	3.47
	1 sun Front + 1 sun Rear	537.3	44.24	45.0	10.71
In + Ga	Front illumination	427.7	17.99	38.9	3.00
	Rear illumination	231.9	4.70	30.9	0.34
	1 sun Front + 1 sun Rear	441.1	22.69	40.7	4.08
In + Ga + In	Front illumination	535.4	21.67	48.8	5.35
	Rear illumination	486.6	11.19	50.2	2.74
	1 sun Front + 1 sun Rear	556.3	33.73	49.6	9.32
Na + In + Ga + In	Front illumination	522.4	21.61	48.9	5.52
	Rear illumination	471.5	12.06	42.8	2.43
	1 sun Front + 1 sun Rear	535.9	32.82	44.3	7.80

When the CIGSe solar cells are measured under simultaneous front and rear illumination, V_{oc}, J_{sc}, and efficiency experience gains compared to front illumination only (Figure 6b and Table 3). The J_{sc} and efficiency under bifacial illumination are close to the sum of the individual front and rear illumination measurements. The *FF* values for the devices with NaF PDT reveal a slight increase under bifacial compared to front illumination only. Just the Na+In+Ga+In CIGSe device shows a drop in *FF*, which may be linked to the high series resistance (Figure S6, Supporting Information). The best Ga+In CIGSe solar cell achieves 10.71% efficiency under 1 sun front + 1 sun rear illumination, which is higher than for the best In+Ga+In CIGSe device (9.32%). The main reason is the lower efficiency of In+Ga+In compared to Ga+In CIGSe under rear illumination, so the higher front illumination efficiency cannot prevail. When the In+Ga+In CIGSe device is measured under rear illumination, the short wavelength light is absorbed in the absorber's bottom region. However, a barrier at 75% depth of the absorber will hinder the electron transport toward the front surface, resulting in a decrease in charge collection. Thus, despite a minimum in In content at the rear interface—as successfully achieved by the In+Ga+In deposition sequence—being beneficial, it is important to restrict it to the immediate vicinity of the back contact.

In Figure 6c, we plot the efficiencies of semi-transparent CIGSe solar cells with various absorber thicknesses (under front illumination) for state-of-the-art devices and our work. The ratios of front-illuminated efficiency/rear-illuminated efficiency (PCE_{Rear}/PCE_{Front}), that is, the bifaciality factors with respect to efficiency, of these CIGSe solar cells are presented in Figure 6d. It is observed that our strategy of first-stage adaptation leaves room for further efficiency enhancement. Regarding the bifaciality, this is still highest for the conventional case of Ga+In (66%). While moving the Ga-peak away from the immediate rear interface is beneficial for the front-illuminated efficiency, the bifaciality factor lags behind with 51% for In+Ga+In and 44% for Na+In+Ga+In. Across the literature, the thin CIGSe solar cells (with absorber thickness below 1 µm) generally reveal higher ratios of PCE_{Rear}/PCE_{Front} than the thick CIGSe solar cells (with absorber thickness above 1 µm). These results indicate that the ultra-thin CIGSe solar cells show potential in agrivoltaics, building-integration, or bifacial operation rather than the standard-thick CIGSe solar cells (with 2–3 µm absorber).

3. Discussion

It is reported that a steep Ga grading toward the rear reduces recombination of the charges at the back contact. Compared to the band gap of $CuInSe_2$, CIGSe shows an increasing band gap with rising Ga content.[11] A Ga-rich rear interface is related to a larger GGI ratio (Figure 2b and Figure 4b), leading to a higher CBM (Figure 2d and Figure 4d).[9a] When the CIGSe absorbers are deposited on both Mo and ITO back contact by the same deposition strategy, they present a similar GGI ratio and band gap gradient. In addition, these CIGSe devices show a similar average visible transmittance (AVT) in the spectral range of 380–770 nm (Figure S8, Supporting Information). Therefore, the semi-transparent CIGSe absorbers (on ITO back contact) are utilized for studying the mechanism of the charge carrier separation and transport.

The schematic diagram of charge carrier transport in these graded CIGSe solar cells is shown in **Figure 7**. When the CIGSe absorber is fabricated with the standard deposition sequence of Ga+In in the first stage, a strong back Ga gradient with a maximum GGI and thus E_g around 90% absorber depth is observed (Figure 4d) and the charge carrier separation explained in Figure 7a: The electrons are repelled from the back interface due to the higher CBM and migrate toward the front surface of the CIGSe absorber (CdS side).[9,10] Simultaneously, the holes can be extracted by the ITO back contact. These considerations confirm that the CIGSe absorber with a steep back Ga gradient leads to a high efficiency due to the effective separation and transport of charge carriers.[9a,10,13]

When In+Ga is deposited in the first stage of the co-evaporation process, the maximum GGI value is located at ≈ 50% of the CIGSe absorber depth (Figure 4b). Therefore, the widest band gap (the highest CBM) is also obtained in this depth of the absorber (Figure 4d and Figure 7b), leading to the formation of a central electron transport barrier.[25] The photo-generated electrons at the bottom region cannot go through that barrier and therefore, serious recombination occurs at the back side of the In+Ga CIGSe absorber. Since the change in VBM with GGI and hence E_g variation is much smaller, the holes are less influenced but tend to be trapped in the region of high GGI and thus are not extracted efficiently either. In other words, the rear interface region of the In+Ga CIGSe solar cell cannot contribute with photo-generated charge carriers to the current generation.

For In+Ga+In and Na+In+Ga+In CIGSe the maximum E_g values are observed at ≈ 75% of the absorber depth (Figure 7c,d). Resulting are increased recombination losses compared to Ga+In CIGSe, following the arguments for In+Ga CIGSe even if the effects are not as pronounced for the later CBM maximum. Both Ga+In and In+Ga+In CIGSe exhibit a narrower band gap value than Na+In+Ga+In CIGSe at the front surface, which is beneficial to form a spike-like band alignment with the CdS buffer layer.[12] Therefore, higher efficiencies are achieved for Ga+In (5.71%) and In+Ga+In (6.18%) CIGSe rather than for Na+In+Ga+In (5.15%), while In+Ga CIGSe leads to significantly lower numbers (Table 2). The highest efficiency is observed for the In+Ga+In CIGSe device owing to the In-rich rear interface and a simultaneous occurrence of the band gap maximum in the second half of the absorber.

To achieve highly efficient semi-transparent CIGSe solar cells, besides the formation of a high back Ga gradient, approaches to avoid GaO_x formation and foster the growth of large grains (as reported for high In content[13]) are essential. The here presented strategy shows that we can to a certain extent move the Ga maximum further inside the absorber without deteriorating the carrier collection. Our results reveal that this approach can be further optimized by minimizing the time of In at the beginning of the first stage while establishing the start with In as a promising strategy for further enhancement of semi-transparent CIGSe solar cells. Therefore, the first stage deposition sequence is crucial for the fabrication of semi-transparent CIGSe solar cell. The silver rear interface modification or sulfurization of the ITO back contact could be alternative strategies for further PV performance improvement.[9b,38]

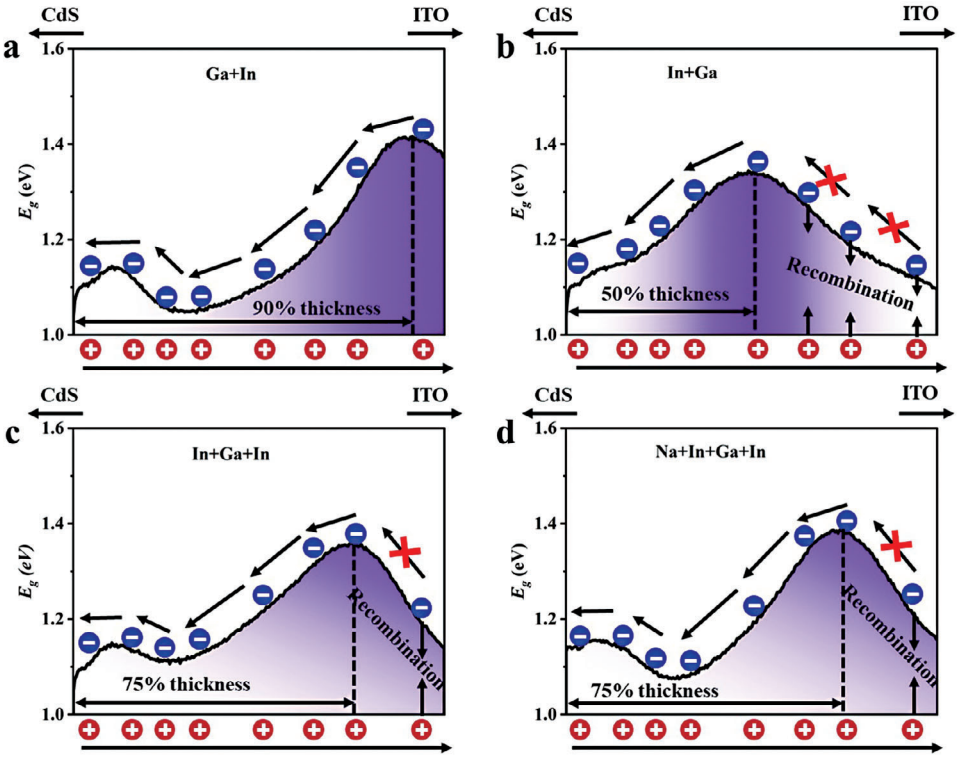

Figure 7. Schematic diagram of charge transport in bandgraded CIGSe absorbers. *x*-axis is the absorber thickness and *y*-axis is the band gap at each depth of CIGSe absorber.

4. Conclusion

We have investigated the PV performance of CIGSe solar cells deposited on ITO and for comparison on Mo back contact by various deposition strategies in the first stage of the co-evaporated absorbers. In particular, we altered the standard deposition sequence of Ga+In to start with In, that is, In+Ga and alternatively In+Ga+In. Additionally, we disclosed the different effects of NaF pre- and post-deposition treatment for the In+Ga+In configuration. An In-rich absorber at the rear interface is desired to enable large grain growth and to avoid GaO_x formation on ITO back contact. At the same time, we revealed that the In-rich phase should be kept to the close vicinity of the back contact to maintain efficient charge carrier transport and extraction. When the CIGSe is deposited on Mo (with Na diffusion barrier), the highest efficiency of 7.57% is observed for CIGSe with Na+In+Ga+In sequence in the first stage. The optimum performance of semi-transparent CIGSe solar cells on ITO is achieved by the deposition of In+Ga+In in the first stage combined with NaF PDT (6.18% efficiency, i.e., 28% on average relatively higher than for the standard deposition sequence Ga+In). Furthermore, this CIGSe solar cell presents an efficiency of 2.74% under rear illumination and 9.32% under simultaneous front and rear irradiance. All in all, starting the first stage of the CIGSe co-evaporation with a short phase of In supply is highly beneficial for enhancing the solar cell performance on Mo and in particular on ITO back contact. This newly introduced modification of the three-stage process of CIGSe growth will open up the doors for efficiency enhancement of semi-transparent devices with multiple applications, for example, in agrivoltaics, building-integration, or bifacial operation.

5. Experimental Section

Materials: Barium-borosilicate glass 7059 (alkali content below 0.3%, purchased from CORNING) is selected to serve as alkali-free glass substrate. 400 nm thick ITO was fabricated in the laboratory onto the glass substrates by DC-sputtering at a rate of 2.5 Å s^{-1} in Ar atmosphere. 800 nm thick Mo with a Si_3N_4 barrier was purchased from PVcomB—Kompetenzzentrum Photovoltaik, Berlin.

Fabrication of CIGSe Absorbers: The sub-500 nm CIGSe absorbers were fabricated on top of Mo or ITO by co-evaporation of the elements (PVD tool Dreva 450). Following the typical three-stage process for CIGSe growth, Se was evaporated continuously during the whole duration of the process, while the fluxes of Cu, In, and Ga were controlled by shutters. Ga and In were provided in the first stage at 410°C substrate temperature to form an In-Ga-Se precursor. After that, the substrate temperature was increased to 450 °C, and Cu was evaporated during the second stage. By the end of the second stage, a Cu-rich thin film [Cu/(Ga+In) = 1.06] had grown owing to the formation of a Cu_xSe phase. This Cu/(Ga+In) ratio was adjusted to 0.85–0.90 by simultaneous evaporation of In and Ga during the third stage. In case of NaF PDT, the Na addition was carried out directly after CIGSe deposition without breaking the vacuum and in a continuous supply of Se. In the experiment, both NaF PDT and NaF Pre-DT were utilized for Na incorporation. For the NaF Pre-DT, NaF plus Se were deposited before the first stage of the absorber deposition. The substrate temperature was kept at 360 °C during the Pre-DT and PDT process.

Fabrication of CIGSe Photovoltaic Devices: On top of the finished absorbers, an 80 nm CdS buffer layer was coated by chemical bath

deposition (CBD). Following, 80 nm intrinsic zinc oxide (i-ZnO) and 300 nm AZO were coated by radio-frequency sputtering. 10 nm Ni and 2000 nm Al contact grids were deposited by thermal evaporation before the samples were mechanically scribed into eight 1 cm × 0.5 cm cells.

Characterization: X-ray fluorescence (XRF, type XEPOS from Spectro) was applied to characterize the absorber thickness (480–495 nm), and average Cu/(Ga+In) (CGI = 0.85–0.90) and Ga/(Ga+In) (GGI = 0.26–0.29) ratio. Glow discharge optical emission spectroscopy (GD-OES, instrument GDA 650HR from Spectruma) measurements were performed for depth-profiling of the CIGSe absorber s, which had been subject to etching in 10% HCl solution for 2 min to remove excessive Na. The current density–voltage (*J–V*) curves were measured for performance evaluation under a standard AM 1.5 G sun simulator at room temperature (type WACOM WXS-10-Super). During the measurement, the samples were kept at a constant temperature of 25 °C via a cooling chuck. The external quantum efficiency (EQE) was measured by a home-built system applying calibrated Si and Ge diodes as references.

Statistical Analysis: As-obtained *J–V* results are imported to an Excel table. Some sub-cells are destroyed during the solar cell fabrication process. Their fill factor values are below 25%, and they are considered outliers. Therefore, the PV performance of these sub-cells is not included in the statistical analysis. The PV performance is presented with (average ± standard deviation) calculated from 10 sub-cells for each experimental recipe.

Supporting Information

Supporting Information is available from the Wiley Online Library or from the author.

Acknowledgements

C.R. and Y.G. contributed equally to this work. The XRF and GD-OES measurements were performed on an instrument funded by the Deutsche Forschungsgemeinschaft (DFG, German Research Foundation)—INST 20876/324-1 FUGG and are acknowledged as follows: "Gefördert durch die Deutsche Forschungsgemeinschaft (DFG)—Projektnummer INST 20876/324-1 FUGG". Y. Gao was financially supported by the Chinese Scholarship Committee. The authors acknowledge support from the Open Access Publication Fund of the University of Duisburg-Essen.

Open access funding enabled and organized by Projekt DEAL.

Conflict of Interest

The authors declare no conflict of interest.

Data Availability Statement

The data that support the findings of this study are available from the corresponding author upon reasonable request.

Keywords

ITO back contact, NaF treatment, semi-transparent, ultrathin $Cu(In,Ga)Se_2$ solar cells

Received: January 26, 2024
Revised: February 28, 2024
Published online:

[1] M. A. Green, E. D. Dunlop, M. Yoshita, N. Kopidakis, K. Bothe, G. Siefer, X. Hao, *Prog. Photovolt.: Res. Appl.* **2023**, *31*, 651.
[2] a) I. Massiot, A. Cattoni, S. Collin, *Nat. Energy* **2020**, *5*, 959; b) C. van Lare, G. Yin, A. Polman, M. Schmid, *ACS Nano* **2015**, *9*, 9603; c) Y. Li, G. Yin, Y. Gao, T. Köhler, J. Lucaßen, M. Schmid, *Sol. Energ. Mat. Sol. C* **2021**, *223*, 110969; d) G. Yin, V. Brackmann, V. Hoffmann, M. Schmid, *Sol. Energ. Mat. Sol. C* **2015**, *132*, 142.
[3] L. M. Mansfield, A. Kanevce, S. P. Harvey, K. Bowers, C. Beall, S. Glynn, I. L. Repins, *Prog. Photovolt.: Res. Appl.* **2018**, *26*, 949.
[4] L. Gouillart, A. Cattoni, W. C. Chen, J. Goffard, L. Riekehr, J. Keller, M. Jubault, N. Naghavi, M. Edoff, S. Collin, *Prog. Photovolt.: Res. Appl.* **2020**, *29*, 212.
[5] Y.-S. Son, H. Yu, J.-K. Park, W. M. Kim, S.-Y. Ahn, W. Choi, D. Kim, J.-H. Jeong, *J. Phys. Chem. C* **2019**, *123*, 1635.
[6] a) G. Yin, M. Song, M. Schmid, *Sol. Energ. Mat. Sol. C* **2019**, *195*, 318; b) T. Schneider, C. Dethloff, T. Hölscher, H. Kempa, R. Scheer, *Prog. Photovolt.: Res. Appl.* **2021**, *30*, 191.
[7] a) J. Chantana, H. Arai, T. Minemoto, *J. App. Phys.* **2016**, *120*, 045302; b) M. J. Shin, A. Lee, A. Cho, K. Kim, S. K. Ahn, J. H. Park, J. Yoo, J. H. Yun, J. Gwak, D. Shin, I. Jeong, J.-S. Cho, *Nano Energy* **2021**, *82*, 105729.
[8] a) Y. Li, S. W. Tabernig, G. Yin, A. Polman, M. Schmid, *Sol. RRL* **2022**, *6*, 2200695; b) D. Kim, S. S. Shin, S. M. Lee, J. S. Cho, J. H. Yun, H. S. Lee, J. H. Park, *Adv. Funct. Mater.* **2020**, *30*, 2001775.
[9] a) W. Witte, D. Abou-Ras, K. Albe, G. H. Bauer, F. Bertram, C. Boit, R. Brüggemann, J. Christen, J. Dietrich, A. Eicke, D. Hariskos, M. Maiberg, R. Mainz, M. Meessen, M. Müller, O. Neumann, T. Orgis, S. Paetel, J. Pohl, H. Rodriguez-Alvarez, R. Scheer, H.-W. Schock, T. Unold, A. Weber, M. Powalla, *Prog. Photovolt.: Res. Appl.* **2015**, *23*, 717; b) S.-C. Yang, T.-Y. Lin, M. Ochoa, H. Lai, R. Kothandaraman, F. Fu, A. N. Tiwari, R. Carron, *Nat. Energy* **2022**, *8*, 40.
[10] S. C. Yang, M. Ochoa, R. Hertwig, A. Aribia, A. N. Tiwari, R. Carron, *Prog. Photovolt.: Res. Appl.* **2021**, *29*, 630.
[11] a) F. Larsson, N. S. Nilsson, J. Keller, C. Frisk, V. Kosyak, M. Edoff, T. Törndahl, *Prog. Photovolt.: Res. Appl.* **2017**, *25*, 755; b) E. Ghorbani, P. Erhart, K. Albe, *Phys. Rev. Mater.* **2019**, *3*, 075401.
[12] G. S. Park, V. B. Chu, B. W. Kim, D.-W. Kim, H.-S. Oh, Y. J. Hwang, B. K. Min, *ACS Appl. Mater. Interfaces* **2018**, *10*, 9894.
[13] J. Dietrich, D. Abou-Ras, T. Rissom, T. Unold, H.-W. Schock, C. Boit, *IEEE J Photovolt* **2012**, *2*, 364.
[14] a) R. Caballero, C. Guillén, M. T. Gutiérrez, C. A. Kaufmann, *Prog. Photovolt.: Res. Appl.* **2005**, *14*, 145; b) R. Klenk, A. Steigert, T. Rissom, D. Greiner, C. A. Kaufmann, T. Unold, M. C. Lux-Steiner, *Prog. Photovolt.: Res. Appl.* **2014**, *22*, 161; c) M. A. Contreras, A. M. Gabor, A. L. Tennant, S. Asher, J. Tuttle, R. Noufi, *Prog. Photovolt.: Res. Appl.* **1994**, *2*, 287.
[15] Y. Gao, G. Yin, M. Schmid, *Adv. Mater.* **2023**, *10*, 2300566.
[16] a) R. Carron, S. Nishiwaki, T. Feurer, R. Hertwig, E. Avancini, J. Löckinger, S.-C. Yang, S. Buecheler, A. N. Tiwari, *Adv. Energy Mater.* **2019**, *9*, 1900408; b) Y. Sun, S. Lin, W. Li, S. Cheng, Y. Zhang, Y. Liu, W. Liu, *Engineering* **2017**, *3*, 452.
[17] P. Salomé, V. Fjällström, A. Hultqvist, M. Edoff, *IEEE J. Photovolt.* **2013**, *3*, 509.
[18] F. Pianezzi, P. Reinhard, A. Chirilă, B. Bissig, S. Nishiwaki, S. Buecheler, A. N. Tiwari, *Phys. Chem. Chem. Phys.* **2014**, *16*, 8843.
[19] a) S. Uličná, L. M. Welch, A. Abbas, M. Togay, V. Tsai, T. R. Betts, A. V. Malkov, J. M. Walls, J. W. Bowers, *Prog. Photovolt.: Res. Appl.* **2021**, *29*, 546; b) Y. Gao, G. Yin, M. Schmid, *Small* **2023**, *19*, 2302581.
[20] Y. Wang, S. Lv, Z. Li, *J. Mater. Sci. Technol.* **2022**, *96*, 179.
[21] a) J. Jiang, R. Giridharagopal, E. Jedlicka, K. Sun, S. Yu, S. Wu, Y. Gong, W. Yan, D. S. Ginger, M. A. Green, X. Hao, W. Huang, H. Xin, *Nano Energy* **2020**, *69*, 104438; b) S. Rehan, J. Moon, T. G. Kim, J. Gwak, J. Kim, J. W. Kim, W. Jo, S. K. Ahn, S. Ahn, *Nano Energy* **2018**, *48*, 401.
[22] H. Elanzeery, F. Babbe, M. Melchiorre, A. Zelenina, S. Siebentritt, *IEEE J. Photovolt.* **2017**, *7*, 684.

[23] a) O. Cojocaru-Mirédin, M. Raghuwanshi, R. Wuerz, S. Sadewasser, *Adv. Funct. Mater.* **2021**, *31*, 2103119; b) J. Matsuura, I. Khatri, T. Y. Lin, M. Sugiyama, T. Nakada, *Prog. Photovolt.: Res. Appl.* **2019**, *27*, 623.
[24] a) M. Bär, W. Bohne, J. Röhrich, E. Strub, S. Lindner, M. C. Lux-Steiner, C. H. Fischer, T. P. Niesen, F. Karg, *J. Appl. Phys.* **2004**, *96*, 3857. b) T. Kodalle, D. Greiner, V. Brackmann, K. Prietzel, A. Scheu, T. Bertram, P. Reyes-Figueroa, T. Unold, D. Abou-Ras, R. Schlatmann, C. A. Kaufmann, V. Hoffmann, *J. Anal. Atom. Spectrom.* **2019**, *34*, 1233.
[25] K. Kim, W. N. Shafarman, *Nano Energy* **2016**, *30*, 488.
[26] a) J. Chantana, Y. Kawano, T. Nishimura, A. Mavlonov, T. Minemoto, *Sol. Energ. Mat. Sol. C* **2020**, *210*, 110502; b) J. Chantana, Y. Kawano, T. Nishimura, Y. Kimoto, T. Kato, H. Sugimoto, T. Minemoto, *ACS Appl. Energy Mater.* **2020**, *3*, 1292. c) M. H. Wolter, R. Carron, E. Avancini, B. Bissig, T. P. Weiss, S. Nishiwaki, T. Feurer, S. Buecheler, P. Jackson, W. Witte, S. Siebentritt, *Prog. Photovolt.: Res. Appl.* **2021**, *30*, 702.
[27] S. Siebentritt, L. Gütay, D. Regesch, Y. Aida, V. Deprédurand, *Sol. Energ. Mat. Sol. C* **2013**, *119*, 18.
[28] M. Mazzer, S. Rampino, G. Spaggiari, F. Annoni, D. Bersani, F. Bissoli, M. Bronzoni, M. Calicchio, E. Gombia, A. Kingma, F. Pattini, E. Gilioli, *Sol. Energ. Mat. Sol. C* **2017**, *166*, 247.
[29] V. B. Chu, S. J. Park, G. S. Park, H. S. Jeon, Y. J. Hwang, B. K. Min, *Korean J. Chem. Eng.* **2016**, *33*, 880.
[30] T. Nishimura, N. Hamada, J. Chantana, A. Mavlonov, Y. Kawano, T. Masuda, T. Minemoto, *ACS Appl. Energy Mater.* **2020**, *3*, 9504.
[31] A. Mavlonov, T. Nishimura, J. Chantana, Y. Kawano, T. Masuda, T. Minemoto, *Sol. Energy* **2020**, *211*, 1311.
[32] T. Nakada, Y. Hirabayashi, T. Tokado, D. Ohmori, T. Mise, *Sol. Energy* **2004**, *77*, 739.
[33] A. Mavlonov, J. Chantana, T. Nishimura, Y. Kawano, M. Inoue, N. Hamada, T. Masuda, T. Minemoto, *Sol. Energy* **2020**, *211*, 725.
[34] M. J. Shin, A. Lee, J. H. Park, A. Cho, S. K. Ahn, D. Shin, J. Gwak, J. H. Yun, J. Yoo, J.-S. Cho, *Nano Energy* **2022**, *92*, 106711.
[35] S. H. Moon, S. J. Park, Y. J. Hwang, D. K. Lee, Y. Cho, D. W. Kim, B. K. Min, *Sci. Rep.* **2014**, *4*, 4408.
[36] Y. Li, G. Yin, M. Schmid, *Sol. Energ. Mat. Sol. C* **2022**, *234*, 111431.
[37] J. Chantana, T. Nishimura, Y. Kawano, N. Suyama, A. Yamada, Y. Kimoto, T. Kato, H. Sugimoto, T. Minemoto, *Adv. Energy Mater.* **2019**, *9*, 1902869.
[38] D. Kim, M. Saifullah, Y. Jo, J. G. An, J.-S. Cho, S. Ahn, J. Gwak, H. S. Lee, J. H. Park, *ACS Appl. Energy Mater.* **2022**, *5*, 10611.